Journal of Maps

ISSN: (Print) 1744-5647 (Online) Journal homepage: https://www.tandfonline.com/loi/tjom20

Allostratigraphy and paleontology of the lower Miocene Chilcatay Formation in the Zamaca area, East Pisco basin, southern Peru

C. Di Celma, P. P. Pierantoni, E. Malinverno, A. Collareta, O. Lambert, W. Landini, G. Bosio, K. Gariboldi, A. Gioncada, C. de Muizon, G. Molli, F. G. Marx, R. M. Varas-Malca, M. Urbina & G. Bianucci

To cite this article: C. Di Celma, P. P. Pierantoni, E. Malinverno, A. Collareta, O. Lambert, W. Landini, G. Bosio, K. Gariboldi, A. Gioncada, C. de Muizon, G. Molli, F. G. Marx, R. M. Varas-Malca, M. Urbina & G. Bianucci (2019) Allostratigraphy and paleontology of the lower Miocene Chilcatay Formation in the Zamaca area, East Pisco basin, southern Peru, Journal of Maps, 15:2, 393-405, DOI: 10.1080/17445647.2019.1604439

To link to this article: https://doi.org/10.1080/17445647.2019.1604439

JOURNAL OF MAPS
2019, VOL. 15, NO. 2, 393–405
https://doi.org/10.1080/17445647.2019.1604439

Science

OPEN ACCESS Check for updates

Allostratigraphy and paleontology of the lower Miocene Chilcatay Formation in the Zamaca area, East Pisco basin, southern Peru

C. Di Celma [a], P. P. Pierantoni [a], E. Malinverno [b], A. Collareta [c], O. Lambert [d], W. Landini [c], G. Bosio [b], K. Gariboldi [c], A. Gioncada [c], C. de Muizon[e], G. Molli [c], F. G. Marx [d,f,g], R. M. Varas-Malca [h], M. Urbina [h] and G. Bianucci [c]

[a]Scuola di Scienze e Tecnologie, Università di Camerino, Camerino, Italy; [b]Dipartimento di Scienze dell'Ambiente e della Terra, Università di Milano-Bicocca, Milano, Italy; [c]Dipartimento di Scienze della Terra, Università di Pisa, Pisa, Italy; [d]D.O. Terre et Histoire de la Vie, Institut Royal des Sciences Naturelles de Belgique, Brussels, Belgium; [e]Centre de Recherche en Paléontologie - Paris - CR2P (CNRS, MNHN, Sorbonne Université), Département Origines et Évolution, Muséum National d'Histoire Naturelle, Paris, France; [f]Paleontology, Museums Victoria, Melbourne, Australia; [g]School of Biological Sciences, Monash University, Clayton, Australia; [h]Departamento de Paleontologia de Vertebrados, Museo de Historia Natural-UNMSM, Lima, Peru

ABSTRACT

Based on mapping of laterally traceable stratigraphic discontinuities, we propose a high-resolution allostratigraphic scheme for one of the world's foremost fossil marine vertebrate Lagerstätten: the lower Miocene strata of the Chilcatay Formation exposed along the Ica River near Zamaca, southern Peru. Measured sections combined with 1:10,000 scale mapping of a 24 km^2 area provide an overview of the stratal architecture, as well as a general facies framework and interpretation of the various depositional settings. As a whole, the Chilcatay alloformation is bounded by the CE0.1 unconformity at the base and the PE0.0 unconformity at the top. An internal Chilcatay surface, termed CE0.2, splits the alloformation into two distinct allomembers (Ct1 and Ct2). The Ct1 allomember comprises three facies associations recording deposition in shoreface, offshore, and subaqueous delta settings. The Ct2 allomember comprises two facies associations, recording deposition in shoreface and offshore settings. Using these data, we place the rich marine vertebrate assemblage in a precise spatial and stratigraphic framework. The well-diversified vertebrate assemblage is dominated by cetaceans (mostly odontocetes) and sharks (mostly lamniforms and carcharhiniforms); rays, bony fish, and turtles are also present. Taxonomic novelties include the first records of baleen whales, platanistids, and eurhinodelphinids from the Chilcatay Formation.

ARTICLE HISTORY
Received 10 January 2019
Revised 2 April 2019
Accepted 3 April 2019

KEYWORDS
Allostratigraphy; facies analysis; vertebrate paleontology

1. Introduction

The infill of the East Pisco Basin (southern Peru) is a globally renowned marine vertebrate Lagerstätte (e.g. Bianucci, Di Celma, Urbina, & Lambert, 2016c, 2018a; Collareta et al., 2015, 2017; Esperante, Brand, Chadwick, & Poma, 2015; Gariboldi et al., 2015; Gioncada et al., 2016, 2018a, 2018b; Lambert et al., 2015, 2017a, 2017b, 2018; Landini et al., 2017a, 2017b; Martinez-Caceres, Lambert, & de Muizon, 2017; Marx, Lambert, & de Muizon, 2017a; Marx et al., 2017b). Despite a long history of research (e.g. Colbert, 1944; de Muizon, 1988; de Muizon & DeVries, 1985), integrated studies elucidating the spatial and stratigraphic distribution of the fossil assemblage have only recently been performed (Bianucci et al., 2016a, 2016b; Brand, Urbina, Chawick, DeVries, & Esperante, 2011; Di Celma et al., 2017). The aim of the latter is to create a firm basis for future geological and paleontological investigations, as well as to encourage the preservation and promotion of this extraordinary paleontological heritage.

Here we present the second of two companion geological maps of the Chilcatay Formation exposed along the Ica River (Di Celma et al., 2018b). This new map focuses on the area of Zamaca (Main Map), which has yielded a rich assemblage of fossil marine vertebrates. The primary objectives of this paper are: (i) to gain a better understanding of stratal geometry and depositional settings of each of the facies associations recognized within the study area; (ii) to place the local fossil assemblage within an accurate spatial and stratigraphic framework; and (iii) to provide a quantitative and qualitative evaluation of marine vertebrate distribution.

2. Geological and stratigraphic settings

The onshore portion of the East Pisco Basin (Figure 1) is over some 30 km wide and about 200 km long, extending approximately from Pisco to Nazca (Dunbar, Marty, & Baker, 1990; León, Aleman, Torres, Rosell, & De la Cruz, 2008; Thornburg & Kulm,

CONTACT C. Di Celma claudio.dicelma@unicam.it Scuola di Scienze e Tecnologie, Geology Section, Via Gentile III da Varano, 1, 62032, Camerino, Italy

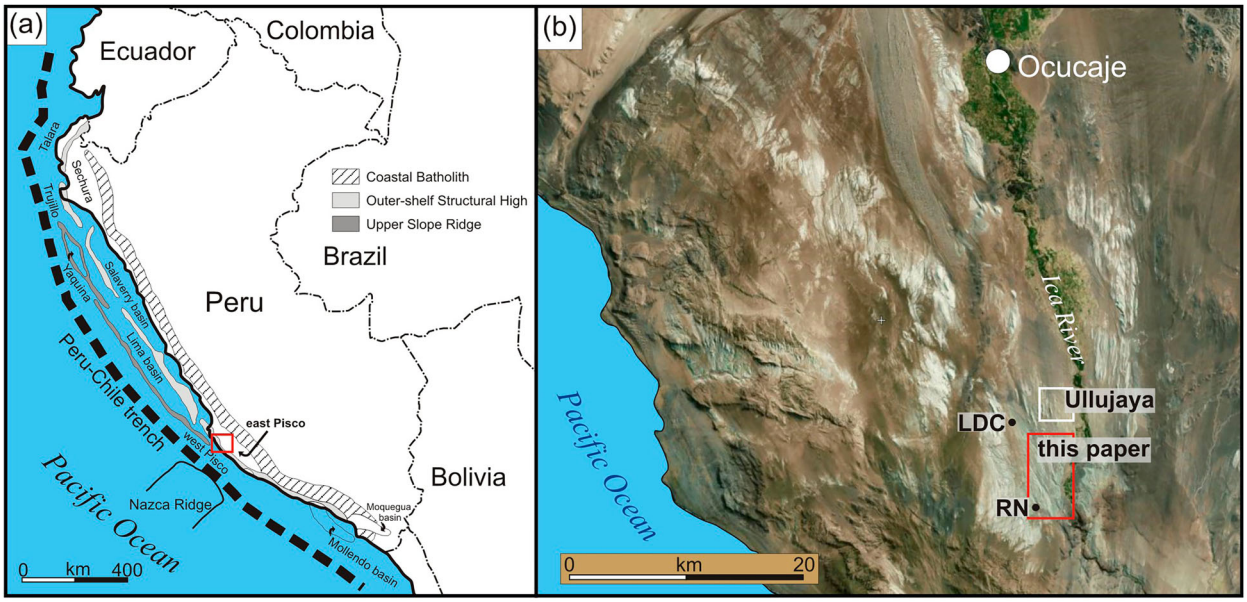

Figure 1. Location maps of the present study. (a) Regional geographic context. The red rectangle outlines location of the area shown in detail in Figure 1(b); (b) annotated air photo image showing locations of the study area (red box). The Chilcatay strata exposed in the area in the white frame (Ullujaya) has been mapped by Di Celma et al. (2018b). Abbreviations for the informal names here used for referring to these otherwise un-named locations: LDC, Los Dos Cerritos; RN, Roca Negra.

1981). The basin started to form not later than the early Eocene (DeVries, 2017) with crustal extension, subsidence, and sediment accommodation probably being driven by subduction-related tectonic erosion (Clift, Pecher, Kukowski, & Hampel, 2003; Hampel, Kukowski, Bialas, & Huebscher, 2004), which also accounts for two major NW-SE and NE-SW trending normal and transtensional fault systems (Rustichelli, Di Celma, Tondi, & Bianucci, 2016a; Rustichelli, Di Celma, Tondi, Baud, & Vinciguerra, 2016b; Viveen & Schlunegger, 2018). Rapid uplift and inversion of the basin started around the latest Pliocene following the subduction of the Nazca Ridge beneath the South America and has persisted to this day (Hsu, 1992; Macharé & Ortlieb, 1992; Saillard et al., 2011).

The basin fill is underlain by Mesozoic and older crystalline and metasedimentary basement rocks (Mukasa & Henry, 1990). Its lithostratigraphic framework was first established by Dunbar et al. (1990) and subsequently refined by DeVries (1998), who

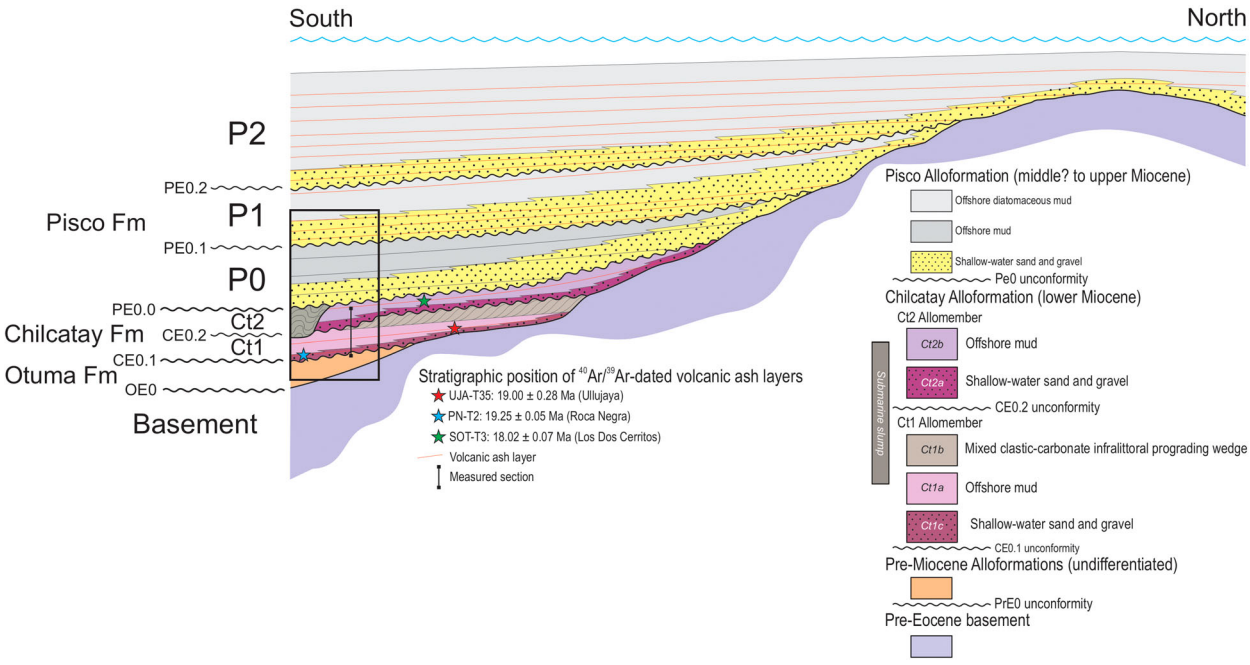

Figure 2. Stratigraphic scheme of the Pisco basin fill along the Ica River. The black box indicates the position of our study area in the scheme.

divided the basin-fill succession into five formations: (i) the Eocene Caballas and Paracas formations, the latter including the Los Choros and Yumaque members (DeVries, 2017); (ii) the uppermost Eocene to lower Oligocene Otuma Formation (DeVries, Urbina, & Jud, 2017); (iii) the upper Oligocene to lower Miocene Chilcatay Formation (DeVries & Jud, 2018); and (iii) the (?)middle Miocene to lower Pliocene Pisco Formation (DeVries & Jud, 2018; Di Celma et al., 2017; Gariboldi et al., 2017).

Because both the base and the top of the Chilcatay Formation are defined by composite unconformities (namely, CE0 and PE0), this lithostratigraphic unit could be more properly regarded as an unconformity-bounded alloformation (NACSN, 2005). A recent regional paleogeographic reconstruction (Di Celma et al., 2018a) shows that, along the Ica River, marine transgression on the bounding unconformities advanced broadly toward the northeast and north, with implied onlap of strata onto the composite CE0 and PE0 transgressive surfaces (Figure 2).

Age constraints for the Chilcatay strata exposed within and nearby the study area are largely based on $^{40}Ar/^{39}Ar$ dating of volcanic ash layers and biostratigraphy. At Ullujaya, about 2.5 km to the north of the study area (Figure 2), an ash layer sampled 2 m above the lowermost available exposure of the Chilcatay Formation (14°35′2.70″S – 75°38′24.80″W) and labeled UJA-T35 yielded an $^{40}Ar/^{39}Ar$ age of 19.00 ± 0.28 Ma (Bosio et al., in press). At Los Dos Cerritos (14°35′41″S–75°40′05″W), an informal name used here for this otherwise unnamed locality (Figure 2), a second ash layer (SOT-T3) located just 1 m below the erosional contact with the overlying Pisco Formation, yielded an $^{40}Ar/^{39}Ar$ age of 18.02 ± 0.07 Ma (Di Celma et al., 2018b), which is consistent with a previous dating of the same tephra by Belia and Nick (2016). Finally, at Roca Negra (Figure 2), a third ash layer sampled 4.5 m above the basal unconformity of the Chilcatay Formation (14°39′2.95″S – 75°38′53.45″W) and labeled PN-T2 yielded an $^{40}Ar/^{39}Ar$ age of 19.25 ± 0.05 Ma (Bosio et al., in press).

A comprehensive micropaleontological study, including both silicoflagellates and diatoms, further constraints the deposition of the local Chilcatay strata between 19 and 18 Ma (Di Celma et al., 2018b; Lambert et al., 2018), thus providing a biostratigraphic framework that is consistent with the aforementioned radiometric ages.

3. Methods

To establish a robust stratigraphic framework for the Chilcatay strata exposed in the fossil-bearing locality of Zamaca, an area covering approximately 24 km^2 was geologically mapped at 1:10.000 scale and a 59 m-thick composite section was logged at decimetre scale. One intraformational unconformity (designated CE0.2) and two laterally persistent packages of coarse-grained beds (designated Ct1-1 and Ct1-2 in ascending order) constitute a basis for stratigraphic correlations throughout the study area and possibly beyond. Sedimentological data collected for paleoenvironmental and stratigraphic interpretations include bed thickness, grain size, grain composition, sedimentary structures, bedding contacts, trace fossils, and the identification of important stratal surfaces. The composite section, which is shown in the supplementary material along with the Main Map, was then used to place new and previous fossil finds into their proper stratigraphic positions.

Vertebrate fossil localities were recorded via a handheld geo-referencing device with a mean horizontal error of less than 10 m. Their stratigraphic position along the measured section was estimated with varying degrees of accuracy, ranging from ± 0.3 to ± 3 m. As for other Miocene fossil-bearing localities of the East Pisco Basin (Bianucci et al., 2016a, 2016b; Di Celma et al., 2018b), most of the detected specimens were examined directly in the field. Only chondrichthyan fossils (teeth and spines) and some particularly notable cetacean specimens have been collected and are now housed at the Museo de Historia Natural de la Universidad Nacional Mayor de San Marcos (MUSM, Lima, Peru). Loose scales of clupeiform fish, which are common finds in some stratal packages at Zamaca, were neither collected nor geo-referenced.

4. The Chilcatay Formation

This study builds on previous stratigraphic work aimed to define the stratal architecture of the Chilcatay and Pisco formations along the western side of the Ica River (Bosio et al., 2019; Di Celma et al., 2016a, 2016b, 2017, 2018a, 2018b). The Chilcatay strata encountered near Zamaca can be divided into two discrete units, informally termed allomember Ct1 and allomember Ct2 from oldest to youngest and defined at base by the CE0.1 and CE0.2 unconformities, respectively. These bounding surfaces converge and merge in marginal areas, i.e. toward the northeast, to form the CE0 composite unconformity.

4.1. CE0.1 unconformity

The base of the Chilcatay Formation is a distinctive angular unconformity (CE0.1) of regional extent that bevels the underlying Otuma Formation (Figure 3 (a)). This surface is delineated by a monospecific suite of the *Glossifungites* Ichnofacies expressed essentially by large *Thalassinoides* that penetrate downward to an average depth of 0.5 m below the discontinuity and are passively filled with medium-grained sand from the overlying *Ct1c* facies association.

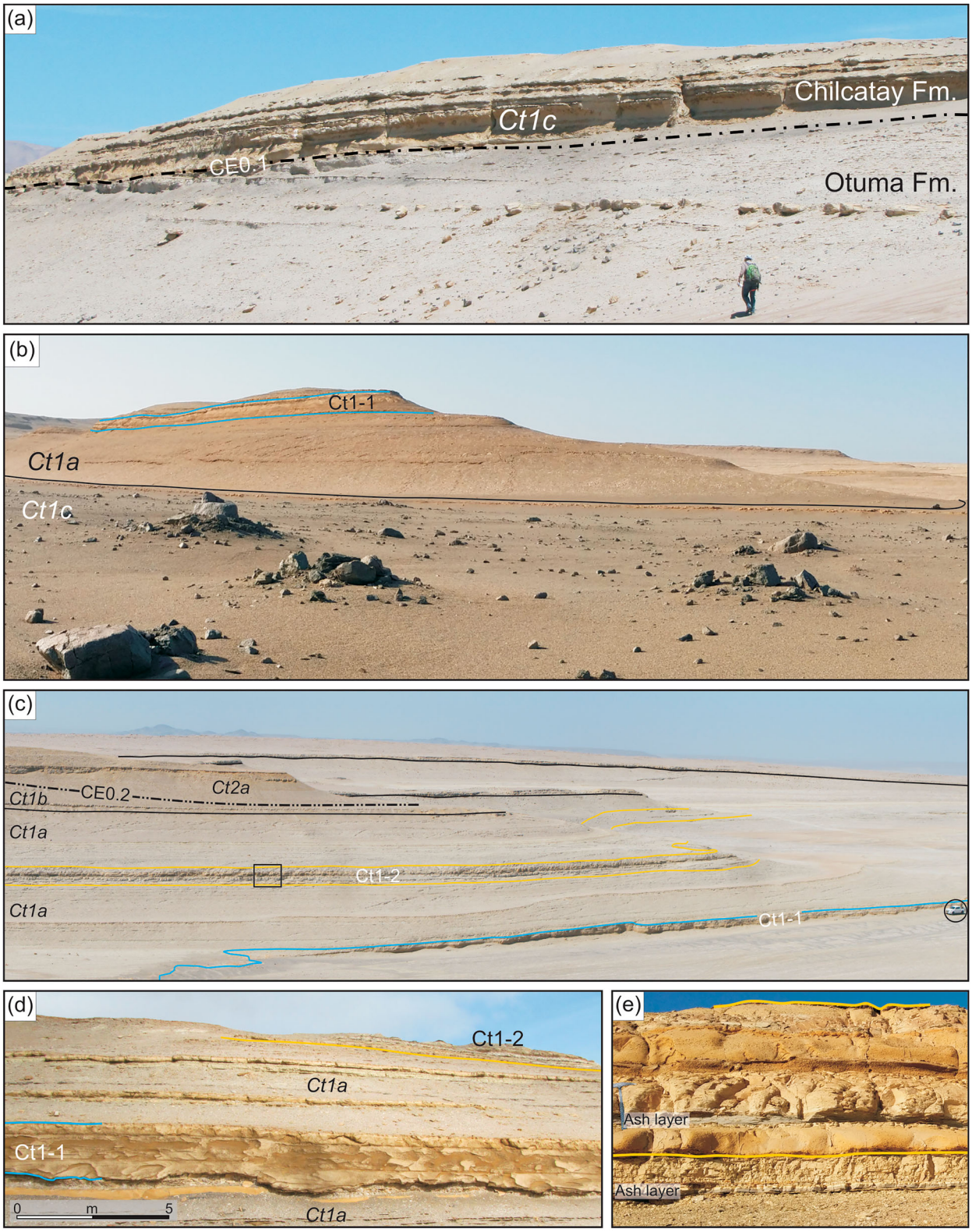

Figure 3. (a) Panoramic view of the angular unconformity (CE0.1) at the base of the Chilcatay Formation (14°38′26″S–75°38′18″W); (b) oblique view of the locality of Zamaca (14°38′3″S–75°38′6″W). Note the presence of outsize boulders protruding above the top of the conglomerate bed into the overlying sandstones; (c) eastward panoramic view of the upper portion of Ct1 (14°37′33″S–75°38′7″W), with an encircled car for scale. Black box indicates position of Figure 3(e); (d) close-up view of Ct1-1 (the two blue lines mark its base and top) sandwiched between finer-grained offshore siltstones (14°37′39″S–75°38′42″W). The basal contact is sharp, extensively scoured and highly irregular; (e) close-up view of the Ct1-2 Marker Unit (the two yellow lines mark its base and top). The association of two different ash layers (a white one and a dark grey one) below and within the Ct1-2 marker bed has been confirmed at different localities by petrographic features.

4.2. Ct1 allomember

This allomember is comprised of three genetically related facies associations. In line with previous work (Coletti et al., 2018; Collareta et al., in press; Di Celma et al., 2018b; Landini et al., 2019), they are designated *Ct1c*, *Ct1a*, and *Ct1b* in upward stratigraphic order. Overall, the Ct1 allomember shows a retrogradational (*Ct1c* and *Ct1a*) to progradational (*Ct1b*) architecture, which indicates sedimentation during rising and stable-to-falling relative sea levels, respectively.

***Ct1c* facies association**: The CE0.1 unconformity is mantled by a lag of well-rounded pebble- to boulder-grade clasts (up to 0.5 m thick) that, in turn, is overlain by a 10 m-thick package of sandstones variably interbedded with lenticular conglomerate beds. Occasional volcanic ash layers occur as thin interbeds. Sandstones are structureless, fine- to medium-grained and may contain varying amounts of granules and small pebbles either scattered or forming lenticular stringers. Conglomerate beds are up to 2.5 m thick and, in general, display poor organization with respect to grain size and bedding. Component clasts, which are locally associated with abundant oyster shells, are mostly derived from the pre-Cenozoic crystalline basement, but also comprise well-rounded clasts of biotite-rich pumice. Outsize clasts up to 2 m in diameter are occasionally observed protruding above the top of the bed into the overlying sandstones (Figure 3(b)). Conglomerates and sandstones typically occur in close vertical association, but locally the entire *Ct1c* consists of sandstones (Figure 3(a)).

The basal conglomerate of the *Ct1c* facies association rests directly above CE0.1 and is interpreted to represent a transgressive lag overlying a wave-ravinement surface (Zecchin, Catuneanu, & Caffau, 2019 and references therein). The overlying conglomeratic sandstones were likely deposited in a shoreface environment, with pervasive bioturbation and the presence of the interbedded conglomerates suggesting highly variable energy conditions (Leithold & Bourgeois, 1984; Zonneveld & Moslow, 2004).

***Ct1a* facies association:** This facies association is 31 m-thick and comprises silty to sandy mudstones interbedded with occasional very fine- to fine-grained sandstone beds up to 0.3 m thick, as well as a few 2–15 cm-thick volcanic ash layers. Invertebrate macrofossils are mostly represented by barnacles, echinoids and bivalves. Within this fine-grained interval there are two laterally extensive packages of coarser grained beds that have been used as stratigraphic datums, namely Ct1-1 and Ct1-2 (Figure 3(c)). These two packages can be easily identified in the outcrops scattered across the study area as they tend to be emphasized by differential weathering of cliff-forming sandstones compared to the surrounding recessive siltstones.

The Ct1-1 marker is about 2.5 m thick and consists of multiple, partially amalgamated, sandstone layers that are arrayed in a fining-upward pattern ranging from medium- to coarse-grained sand at the base, locally containing abundant skeletal debris (most notably barnacles), to fine-grained sand at the top. In places, these sandstone layers pass laterally into discontinuous conglomerate beds that may constitute a substantial portion of the sediment. Conglomerates are composed of a variable mixture of basement-derived pebble- to boulder-grade clasts, and well-rounded pebble- to cobble-grade clasts of biotite-rich pumice. Outsize clasts are common and reach diameters of more than 3 m. Basement-derived clasts are dominantly angular to sub-angular, but a minor amount of subrounded to well-rounded elements also occur. The basal contact of the lower layer is sharp and continuous with broad (up to 1.5 m in cross section) and shallow (0.5 m deep) erosional scours into the underlying siltstones (Figure 3(d)). Beds of this package include a fauna of starfish, ophiuroids, sea urchins, and crinoids, as well as oysters described by DeVries and Jud (2018) and are anomalously rich in both articulated and disarticulated skeletal elements from sharks, marine mammals, and other marine vertebrates.

The Ct1-2 marker is about 2.5 m thick and consists of tabular, laterally extensive beds of light brown (weathering to yellow), fine- to medium-grained sandstones ranging in thickness from 0.4 to 0.5 m, interbedded with a whitish, 0.5 m-thick siltstone bed and a gray-yellowish, 15 cm-thick volcanic ash layer (Figure 4(a)). The sandstone beds are massive and their tops intensely bioturbated by vertically spiraling *Gyrolithes* burrows.

Within *Ct1a*, ash layers are white in color except one being dark gray. They are composed of >95% of glass shards, few juvenile feldspar and occasional amphibole and biotite. Glass shards are colorless, fine-grained, with platy and minor stretched morphology, while in the dark grey tephra they are brownish.

We interpret the fine-grained sediments of *Ct1a* as background deposition in a low-energy offshore setting, where continuous accumulation of fine material via suspended fallout deposition was interrupted only by the deposition of occasional, thin sandstone beds likely related to offshore-directed, storm-generated currents (tempestites) (e.g. Aigner & Reineck, 1982).

We concur with DeVries and Jud (2018) in interpreting the coarse-grained layers of Ct1-1 as the result of tsunami backwash processes that entrained and transported in the offshore setting a mixture of skeletal sand and gravel from nearby shoreface, beach, and landward erosion areas (e.g. Cantalamessa & Di Celma, 2005; Einsele, 1998). Distinguishing characteristics include: (i) the highly irregular basal erosion surfaces with multiple asymmetric and symmetric scours; (ii) the unusually coarse grain-size in comparison with

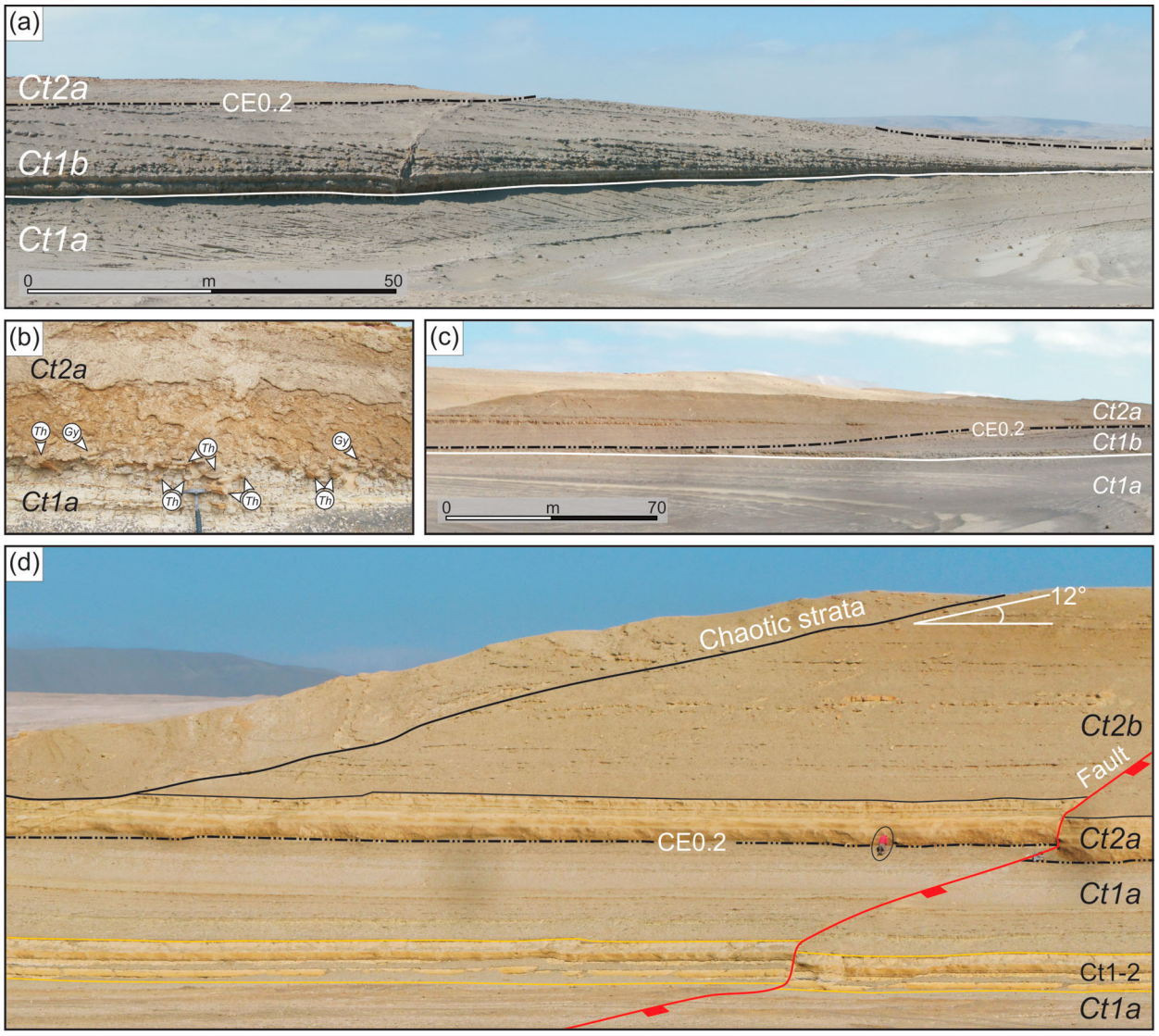

Figure 4. (a) Southeastward panoramic view of *Ct1b* (14°37′25″S–75°38′10″W). The clinoforms show sigmoidal and less commonly tangential downlap onto the underlying *Ct1a*, whereas the tops are partially truncated by the CE0.2 unconformity; (b) close-up of the burrowed firmground (CE0.2) at the base of Ct2 (14°37′1″S 75°38′48″W), penetrated by large *Thalassinoides* (*Th*) and *Gyrolithes* (*Gy*) documenting a *Glossifungites* ichnofacies (30-cm-long hammer for scale). Note that the brownish, shark-tooth rich sand from the mantling *Ct2a* is piped down into these burrows and into the underlying light-gray weathering siltstones of *Ct1a*; (c) northwestward panoramic view (14°37′22″S–75°38′14″W), showing clinobeds toeing out asymptotically on the underlying *Ct1a* siltstones and rapidly wedging out basinwards (to the left); (d) panoramic view of the regularly-bedded upper portion of Ct1 and the lower portion of Ct2, which is cut by a southwest-dipping sharp surface overlain by variably deformed strata (14°37′4″S–75°38′48″W). Downwards, the surface becomes less distinct and passes into a sheared interval zone comprising numerous extensional faults with throws of 0.1–0.5 m in the immediately underlying undeformed sandstones of *Ct2a*. The concave shape and gradient of the basal surface indicate a position at the lateral (eastern) margin of a submarine landslide. Encircled geologist for scale.

the encasing background sediments; (iii) the absence of internal bioturbation; (iv) the presence of multiple graded beds; and (v) the admixture of both well-rounded and angular clasts derived from nearshore and subaerial coastal areas, respectively. The preservation potential of tsunami deposits in offshore settings is facilitated by their emplacement below storm wave base, where they cannot be modified by typical waves. Alternative interpretations of these deposits as the result of extreme weather events are contradicted by the occurrence of outsize boulders too large to be transported seaward any significant distance by even the most violent storm surges. Based on the enormous abundance of vertebrate skeletal remains encased in these deposits relative to adjacent strata, we suggest that these animals fell victim of this catastrophic event, mirroring the way dead fish, turtles, and dolphins are often strewn across the landscape following modern tsunamis (Chagué-Goff, Schneider, Goff, Dominey-Howes, & Strotz, 2011).

The sandstone beds of Ct1-2 are interpreted as tempestites resulting from exceptionally severe storm events transporting shoreface-derived sand-sized sediment into the offshore environment. Upon deposition, these distal storm deposits were colonized and partially reworked during fair-weather conditions by opportunistic

organisms favoring sandy substrates (e.g. Pemberton & MacEachern, 1997).

***Ct1b* facies association:** This facies association is comprised of a southwesterly prograding wedge characterized by oblique and sigmoidal clinoforms downlapping onto the underlying sediments of *Ct1a* (Figure 4(a)). This wedge extends about 4 km downdip and its thickness decreases basinwards from about 20 m in the northeastern portion of the study area to a zero-edge in its central part. Updip, the foresets are truncated by the overlying CE0.2 unconformity and topsets are poorly preserved or absent, whereas downdip they pass asymptotically into bioturbated toesets and bottomsets (Figure 4(a)). Individual foresets are between 0.2 and 0.5 m thick, have dip angle ranging between 15° and 20°, and include a variable mixture of coarse-grained biogenic components, like barnacles, mollusks, echinoids, and calcareous tubes, as well as granule- and small pebble-sized terrigenous components.

Stratal architecture, bedding patterns, and composition of the *Ct1b* clinoforms strikingly resemble those of subaqueous deltas developed in mixed temperate carbonate–siliciclastic systems (Hansen, 1999; Massari & D'Alessandro, 2012; Pomar & Tropeano, 2001). In such deltas, the accommodation space is limited by the dominant oceanographic regime (physical accommodation space *sensu* Pomar & Kendall, 2008), resulting in the bulk of the sediment bypassing the submerged topsets and depositing on the clinoform slope through the combined action of storm-related waves and downwelling bottom currents. Fully carbonate and siliciclastic counterparts of the mixed siliciclastic–carbonate *Ct1b* facies association documented here have been described by Pomar, Aurell, Bádenas, Morsilli, & Al-Awwad (2015) (oolitic infralittoral prograding wedge), Hernández-Molina et al. (2000) (infralittoral prograding wedge), Cattaneo, Correggiari, Langone, and Trincardi (2003) (mud-rich subaqueous wedge), and Patruno, Hampson, Jackson, and Dreyer (2015) (sand-rich subaqueous delta).

4.3. CE0.2 unconformity

Seaward of the basinal pinch out of *Ct1b*, the CE0.2 unconformity is interpreted at an abrupt basinward dislocation of facies belts, with sediments of a shallower setting (*Ct2a*) resting directly on sediments of a deeper setting (*Ct1a*). This surface is commonly recognized through the presence of large, passively infilled *Thalassinoides* and *Gyrolithes* burrows extending into underlying silts of *Ct1a* (Figure 4(b)). When traced landward, CE0.2 directly overlies *Ct1b* (Figure 4(c)) and is typically penetrated by *Thalassinoides*. Despite its abrupt nature, considerable lateral extent, and the presence of locally derived rip-up clasts (see below), CE0.2 exhibits only minor erosional relief across the scale of the outcrop and is interpreted as cut during lowstand subaerial exposure and subsequently reworked by marine ravinement during transgression.

4.4. Ct2 allomember

Two genetically related facies associations have been identified in this allomember. They are designated *Ct2a* and *Ct2b* in ascending order and indicate deposition in nearshore to offshore settings during renewed relative sea level rise and transgression.

***Ct2a* facies association:** This facies association is about 3.5 m thick and lies both sharply and unconformably above the fine-grained sediments of *Ct1a* in distal positions (Figure 4(b)), and the erosional top of *Ct1b* in proximal positions (Figures 4(a) and 4(c)). It is composed of highly fossiliferous, medium- to very coarse-grained sandstones (Figure 4(b)) containing sub-rounded to sub-angular pebbles derived from the immediately underlying siltstones, as well as basement derived clasts and rare coal fragments scattered along the base. Biogenic reworking is extremely pronounced and results in a generally massive bedding appearance. The fossil content comprises dispersed crustaceans (crabs and barnacles), shark teeth and vertebrae (Landini et al., 2019).

Considering the intensity of bioturbation and lack of primary sedimentary structures, we propose that *Ct2*a was deposited in a weak-energy shoreface setting (MacEachern & Pemberton, 1992), marking the local onset of a regionally extensive marine transgression.

***Ct2b* facies association:** This facies association is more than 15 m-thick and comprises a heterolithic succession of weakly bioturbated, thinly-bedded silty mudstone intercalated with minor, laterally persistent, very fine-grained sandstone interbeds and occasional volcanic ash layers.

Over most of the study area, *Ct2b* comprises gently dipping to flat-lying beds. Along the western side of the study area, however, a package characterized by significant internal distortion and deformation of bedding is exposed. This internally deformed package is underlain by a distinct, scoop-shaped surface that cuts to varying degrees into the underlying undeformed succession. At its most eastward exposure (Figure 4(d)), this surface exhibits at least 15 m of incision into *Ct2b*. Towards the west it extends beneath the level of the CE0.2 unconformity, cutting through the Ct1-2 marker and attaining a total depth of incision of at least 30 m. Yet further west, it passes into the subcrop, such that the deepest point of erosion is not exposed.

Overall, the fine-grained nature of *Ct2b* reflects deposition in an offshore setting, where silty mudstones were deposited from suspension during fair-weather periods, and sandstone tempestite beds were deposited by occasional storms (Aigner & Reineck, 1982); supporting this interpretation, clupeiform scales and diatoms are frequently found in the *Ct2b* strata,

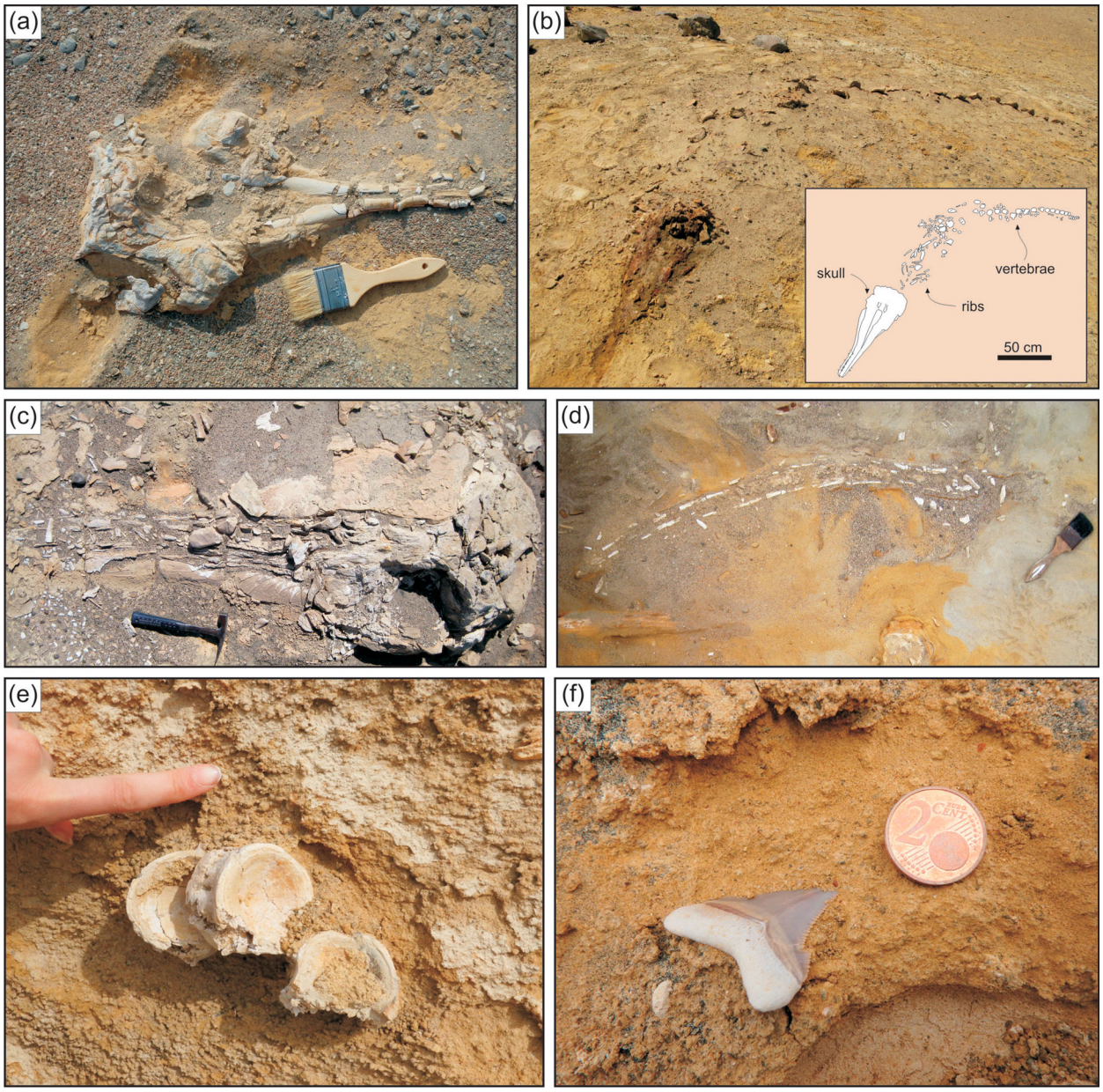

Figure 5. Fossil vertebrates from the Chilcatay strata exposed at Zamaca. (a) Isolated skull of *Notocetus* sp. (squalodelphinid, toothed whale) in anterodorsolateral view, *Ct1c*; (b) articulated skeleton of the holotype of *Inticetus vertizi* (inticetid, toothed whale) with the skull in anterodorsal view, *Ct1c*; (c) skull of indeterminate baleen whale in dorsal view, *Ct2b*; (d) plan view of the mandible of an indeterminate baleen whale in dorsal or ventral view, *Ct1c*; (e) vertebrae of indeterminate large-sized lamniform (shark), *Ct2a*, ShB-4; (f) tooth of *Carcharocles chubutensis* (shark), *Ct2a*, ShB-4.

thus suggesting an epipelagic-neritic paleoenvironment (see also DeVries & Jud, 2018 at this respect). Because the internally deformed sediment wedge is underlain by undeformed strata and is separated from the laterally adjacent undeformed strata by a sharp concave-upward surface, we here interpret it as the result of submarine slumping with remobilization of primary bedding and ductile deformation of the strata.

5. Vertebrate paleontology

In total, we recorded 140 individual marine vertebrate fossils inside the study area, distributed throughout the 59 m-thick section of the Chilcatay Formation. Of the 129 specimens whose stratigraphic level could be determined, 25 were found in *Ct1c*, 95 in *Ct1a* (54, or 41.9% of the total assemblage, in Ct1-1), 2 in *Ct1b*, 6 in *Ct2a*, and 1 in *Ct2b* (see Main Map).

As at the nearby locality of Ullujaya (Bianucci et al., 2018b), fossils are mostly incomplete and either partially or fully articulated, albeit with some notable exception (e.g. Lambert et al., 2018). Cetacean remains dominate the assemblage (79.9%). Curiously, there are just two baleen whales (Mysticeti; Figures 5(c) and 5(d)), with all other specimens identified as belonging to either echolocating toothed cetacean (Odontoceti) or, in cases where only vertebrae and/or ribs were preserved, aff. Odontoceti.

Excluding indeterminate remains (43.6%), odontocetes are represented by Kentriodontidae (19.5%),

Physeteroidea (5.4%), Squalodelphinidae (5.4%), Platanistidae (1.3%), other Platanistoidea (0.7%), Eurhinodelphinidae (1.3%), the archaic heterodont odontocete *Inticetus vertizi* (0.7%), and the long-snouted homodont odontocete *Chilcacetus cavirhinus* (0.7%).

Most of the kentriodontids (including 12 specimens now kept at MUSM) belong to *Kentriodon* sp., which also occurs at Ullujaya. Physeteroids include a well-preserved skull with an unusually narrow and elongated rostrum bearing relatively small teeth. Together with other skulls observed at Zamaca and the two physeteroid specimens collected at Ullujaya (Bianucci et al., 2018b), the new fossil reveals an unexpectedly high degree of sperm whale disparity in the Chilcatay assemblage. Squalodelphinids are represented by remains resembling *Notocetus vanbenedeni* (Figure 5(a)) and *Huaridelphis raimondii* (including MUSM 599 and MUSM 603, described by Lambert et al., 2010). Platanistids are tentatively recorded for the first time in the Chilcatay Formation, and include a rostrum with associated mandibles (MUSM 631) and a partial skeleton including the skull. Similarly, eurhinodelphinids are also identified for the first time here, and comprise a partial skull (MUSM 632), as well as an uncollected skull with associated cervicals. The heterodont dolphin *Inticetus vertizi* is known only from the holotype (MUSM 1980; Figure 5(b)), an almost complete skeleton found at the base of the Chilcatay section at Roca Negra (Lambert et al., 2018). Finally, *Chilcacetus cavirhinus* is represented by a skull with associated postcrania (MUSM 2527), collected about 10 m above the base of the measured section (abs). This specimen is now under study, along with additional material from Ullujaya.

Bony fish represent 11.5% of the marine vertebrate assemblage, and are distributed between 10 and 22.4 m abs. They are represented by fragmentary skeletons, consisting of large cranial and postcranial bones, including some tuna-like vertebrae and two istiophorid-like billfish skulls (in addition to these records, it should be noted that loose clupeiform scales are widespread in the fine-grained sediments of *Ct1a* and *Ct2b*, suggesting the presence of schools of epipelagic fish in the early Miocene offshore paleoenvironments of Zamaca). Disarticulated elasmobranch vertebrae are present, but uncommon (2%). Marine turtles (6%) were found from 7 m to 47.2 m abs, and include an almost complete skeleton, some skulls (one of which collected), and some more fragmentary specimens. Most of these bones are large, and could plausibly represent the same dermochelyid as recorded at Ullujaya (Bianucci et al., 2018b).

We collected more than four thousand elasmobranch teeth and spines from the northern portion of the study area, representing at least twenty-two species in five orders of sharks and rays (Landini et al., 2019). The elasmobranch remains concentrate in four intervals, designated ShB-1 to ShB-4 in ascending stratigraphic order. Of these, ShB-1 and ShB-2 are located within *Ct1a*, and specifically coincide with Ct1-1 and Ct1-2; ShB-3 is situated at the top of the *Ct1b* clinoforms; and ShB-4, which accounts for more than half of the detected specimens (Figures 5(e) and 5(f)), is found at the base of *Ct2a*. Integrating the data of Landini et al. (2019) with further observations from other sites within the study area (including Roca Negra) reveals an elasmobranch assemblage comprising Carcharhiniformes (48.7%, including carcharhinids, sphyrnids, and hemigaleids), Lamniformes (47.8%, including lamnids, otodontids, alopiids, odontaspidids, and megachasmids), Myliobatiformes (3.3%, including myliobatoids and dasyatids), Rhinopristiformes (<0.1%, pristids only), and Squatiniformes (<0.1%, squatinids only). *Carcharhinus brachyurus* and *Cosmopolitodus hastalis* are the dominant taxa, and together account for more than 60% of the recorded specimens.

6. Conclusions

We present a comprehensive overview of the stratigraphic architecture, depositional settings, and vertebrate paleontology of the lower Miocene Chilcatay strata exposed at Zamaca (East Pisco Basin, southern Peru). The allostratigraphic scheme originally established for the Chilcatay Formation at Ullujaya is extended southwards into the Zamaca area, where the intraformational CE0.2 unconformity subdivides the exposed succession into two allostratigraphic units (Ct1 and Ct2 allomembers). The Ct1 allomember comprises three facies associations recording deposition in shoreface (*Ct1c*), offshore (*Ct1a*), and a mixed siliciclastic–carbonate subaqueous delta (*Ct1b*) perched on the basin margin. Two coarse-grained packages, Ct1-1 and Ct1-2, have been traced across the study area within the fine-grained *Ct1a* facies association. The Ct2 allomember comprises two facies associations recording deposition in shoreface (*Ct2a*) and offshore (*Ct2b*) settings.

This work provides both a quantitative and qualitative account of marine vertebrate distribution in a fossil rich early Miocene marine locality, with individual fossils being located precisely on a high-resolution geological map and accompanying stratigraphic section. Fossils are unevenly distributed and especially concentrated within Ct1-1, a possible tsunami deposit. The Zamaca vertebrate assemblage is dominated by cetaceans (mostly toothed whales) and sharks (mostly lamniforms and carcharhiniforms); ray, bony fish and turtles are also present. Its overall composition resembles that of the coeval assemblage at Ullujaya, yet also provides the first record of baleen whales, platanistids, and eurhinodelphinids from the Chilcatay Formation.

Software

The geological map was compiled by scanning hand drafts as black and white TIF files, and then digitizing the line art using the Corel Draw X3 graphics package. We used the GIS Data processing application Global Mapper 12 to generate contour lines for the 1:10,000 scale topographic base map. To do so, we relied on digital elevation model (DEM) based on the Shuttle Radar Topography Mission 26 (SRTM), as released by the United States Geological Survey (SRTM3 USGS version 2.1). The background aerial imagery is from World Imagery (Esri, https://services.arcgisonline.com/ArcGIS/rest/services/World_Imagery/MapServer).

Acknowledgements

We thank W. Aguirre, E. Díaz, R. Salas-Gismondi., M. Martínez-Cáceres, K. Post, and J. Tejada for their help during fieldwork, as well as W. Aguirre for fossil preparation and R. Salas-Gismondi for providing assistance during our stays at the MUSM. Journal reviewers G. Coletti, T.J. DeVries, M. Murad-al-shaikh, and Associate Editor Monica Pondrelli are gratefully acknowledged for their thoughtful contribution and helpful criticism that sharpened the focus of this study. We also thank T.J. DeVries for providing invaluable guidance to new field sites and insightful discussions; responsibility for facts and interpretations nevertheless remains with the authors. The field prospections were made under the auspices of a collaborative program between the Museo de Historia Natural of the Universidad Nacional Mayor de San Marcos (Lima, Peru) and several research institutions. All specimens collected as part of this project have been deposited at the Museo de Historia Natural.

Disclosure statement

No potential conflict of interest was reported by the authors.

Funding

Fieldwork was supported by grants from the Italian Ministero dell'Istruzione, dell'Università e della Ricerca (MIUR) to Bianucci (PRIN Project, 2012YJSBMK EAR- 9317031), Malinverno (PRIN Project, 2012YJSBMK_002), Di Celma (PRIN Project, 2012YJSBMK_003; FFABR 2017 grant); National Geographic Society Committee for Research Exploration to Bianucci [grant number 9410-13] and Lambert [grant number GEFN177-16]; the University of Pisa to Bianucci (PRA_2017_0032); European Commission Marie Skłodowska-Curie Global Postdoctoral fellowship to Marx (656010/MYSTICETI); Università di Pisa

ORCID

C. Di Celma http://orcid.org/0000-0001-7781-7981
P. P. Pierantoni http://orcid.org/0000-0002-1237-4689
E. Malinverno http://orcid.org/0000-0002-9124-5155
A. Collareta http://orcid.org/0000-0002-6513-8882
O. Lambert http://orcid.org/0000-0003-0740-5791
W. Landini http://orcid.org/0000-0001-7196-9888
G. Bosio http://orcid.org/0000-0001-8067-4926
K. Gariboldi http://orcid.org/0000-0002-7978-7496
A. Gioncada http://orcid.org/0000-0002-8513-7377
G. Molli http://orcid.org/0000-0001-9488-8132
F. G. Marx http://orcid.org/0000-0002-1029-4001
R. M. Varas-Malca http://orcid.org/0000-0002-4435-8229
M. Urbina http://orcid.org/0000-0002-1898-9051
G. Bianucci http://orcid.org/0000-0001-7105-0863

References

Aigner, T., & Reineck, H. E. (1982). Proximality trends in modern sands from the Heligoland Bight (North Sea) and their implications for basin analysis. *Senckenbergiana Maritima*, *14*, 183–215.

Belia, E. R., & Nick, K. E. (2016). Early-Miocene calcareous nannofossil biostratigraphy from low-latitude, Pisco Basin, Peru. *Geological Society of America, Abstracts with Programs*, *48*, 4.

Bianucci, G., Bosio, G., Malinverno, E., de Muizon, C., Villa, I. M., Urbina, M., & Lambert, O. (2018a). A new large squalodelphinid (Cetacea, Odontoceti) from Peru sheds light on the early miocene platanistoid disparity and ecology. *Royal Society Open Science*, *5*, Article number 172302. doi:10.1098/rsos.172302

Bianucci, G., Collareta, A., Bosio, G., Landini, W., Gariboldi, K., Gioncada, A., … Di Celma, C. (2018b). Taphonomy and palaeoecology of the lower Miocene marine vertebrate assemblage of Ullujaya (Chilcatay Formation, East Pisco Basin, southern Peru). *Palaeogeography, Palaeoclimatology, Palaeoecology*, *511*, 256–279. doi:10.1016/j.palaeo.2018.08.013

Bianucci, G., Di Celma, C., Collareta, A., Landini, W., Post, K., Tinelli, C., … Lambert, O. (2016a). Fossil marine vertebrates of Cerro Los Quesos: Distribution of cetaceans, seals, crocodiles, seabirds, sharks, and bony fish in a late Miocene locality of the Pisco Basin, Peru. *Journal of Maps*, *12*, 1037–1046. doi:10.1080/17445647.2015.1115785

Bianucci, G., Di Celma, C., Landini, W., Post, K., Tinelli, C., de Muizon, C., … Lambert, O. (2016b). Distribution of fossil marine vertebrates in Cerro Colorado, the type locality of the giant raptorial sperm whale *Livyatan melvillei* (Miocene, Pisco Formation, Peru). *Journal of Maps*, *12*, 543–557. doi:10.1080/17445647.2015.1048315

Bianucci, G., Di Celma, C., Urbina, M., & Lambert, O. (2016c). New beaked whales from the late Miocene of Peru and evidence for convergent evolution in stem and crown Ziphiidae (Cetacea, Odontoceti). *PeerJ*, *4*, e2479. doi:10.7717/peerj.2479

Bosio, G., Gioncada, A., Malinverno, E., Di Celma, C., Villa, I. M., Cataldi, G., … Bianucci, G. (2019). Chemical and petrographic fingerprinting of volcanic ashes as a tool for high-resolution stratigraphy of the upper Miocene Pisco Formation (Peru). *Journal of the Geological Society, London*, *176*, 13–28. doi:10.1144/jgs2018-071

Bosio, G., Malinverno, E., Villa, I. M., Di Celma, C., Gariboldi, K., Gioncada, A., … Bianucci, G. (in press). Tephrochronology and chronostratigraphy of the Miocene Chilcatay and Pisco formations (East Pisco Basin, Peru). *Newsletters on Stratigraphy*.

Brand, L. R., Urbina, M., Chawick, A., DeVries, T. J., & Esperante, R. (2011). A high resolution stratigraphic framework for the remarkable fossil cetacean assemblage of the Miocene/Pliocene Pisco Formation, Peru. *Journal of South American Earth Sciences*, *31*, 414–425. doi:10.1016/j.jsames.2011.02.015

Cantalamessa, G., & Di Celma, C. (2005). Sedimentary features of tsunami backwash deposits in a shallow marine Miocene setting, Mejillones Peninsula, northern Chile. *Sedimentary Geology*, *178*, 259–273. doi:10.1016/j.sedgeo.2005.05.007

Cattaneo, A., Correggiari, A., Langone, L., & Trincardi, F. (2003). The late-Holocene Gargano subaqueous delta, Adriatic shelf: Sediment pathways and supply fluctuations. *Marine Geology*, *193*, 61–91. doi:10.1016/S0025-3227(02)00614-X

Chagué-Goff, C., Schneider, J.-L., Goff, J. R., Domineyhowes, D., & Strotz, L. (2011). Expanding the proxy toolkit to help identify past events — Lessons from the 2004 Indian Ocean Tsunami and the 2009 South Pacific Tsunami. *Earth-Science Reviews*, *107*, 107–122. doi:10.1016/j.earscirev.2011.03.007

Clift, P. D., Pecher, I., Kukowski, N., & Hampel, A. (2003). Tectonic erosion of the Peruvian forearc, Lima Basin, by subduction and Nazca Ridge collision. *Tectonics*, *22*, 1023. doi:10.1029/2002TC001386

Colbert, E. H. (1944). A new fossil whale from the Miocene of Peru. *Bulletin of the American Musem of Natural History*, *83*, 195–216.

Coletti, G., Bosio, G., Collareta, A., Buckeridge, J. S., Consani, S., & El Kateb, A. (2018). Palaeoenvironmental analysis of the Miocene barnacle facies: Case studies from Europe and South America. *Geologica Carpathica*, *69*(6), 573–592. doi:10.1515/geoca-2018-0034

Collareta, A., Coletti, G., Bosio, G., Buckeridge, J., de Muizon, C., DeVries, T. J., … Bianucci, G. (in press). A new barnacle (Cirripedia: Neobalanoformes) from the early Miocene of Peru: Palaeoecological and palaeobiogeographical implications. *Neues Jahrbuch für Geologie und Paläontologie, Abhandlungen*, in press.

Collareta, A., Landini, W., Chacaltana, C., Valdivia, W., Altamirano-Sierra, A., Urbina-Schmitt, M., & Bianucci, G. (2017). A well preserved skeleton of the fossil shark *Cosmopolitodus hastalis* from the late Miocene of Peru, featuring fish remains as fossilized stomach contents. *Rivista Italiana di Paleontologia e Stratigrafia*, *123*, 11–22. doi:10.13130/2039-4942/8005

Collareta, A., Landini, W., Lambert, O., Post, K., Tinelli, C., Di Celma, C., … Bianucci, G. (2015). Piscivory in a Miocene Cetotheriidae: First record of fossilized stomach content for an extinct baleen-bearing whale. *The Science of Nature*, *102*, 70. doi:10.1007/s00114-015-1319-y

de Muizon, C. (1988). Les Vertébrés de la Formation Pisco (Pérou). Troisième partie: Les Odontocètes (Cetacea, Mammalia) du Miocène. *Travaux de l'Institut Français d'Études Andines*, *42*, 1–244.

de Muizon, C., & DeVries, T. J. (1985). Geology and paleontology of late Cenozoic marine deposits in the Sacaco area (Peru). *Geologische Rundschau*, *74*, 547–563. doi:10.1007/BF01821211

DeVries, T. J. (1998). Oligocene deposition and Cenozoic sequence boundaries in the Pisco Basin. *Journal of South American Earth Sciences*, *11*, 217–231. doi:10.1016/S0895-9811(98)00014-5

DeVries, T. J. (2017). Eocene stratigraphy and depositional history near Puerto Caballas (East Pisco Basin, Peru). *Boletín de la Sociedad Geológica del Perú*, *112*, 39–52.

DeVries, T. J., & Jud, N. A. (2018). Lithofacies patterns and paleogeography of the Miocene Chilcatay and lower Pisco depositional sequences (East Pisco Basin, Peru). *Boletín de la Sociedad Geológica del Perú*, *8*, 124–167.

DeVries, T. J., Urbina, M., & Jud, N. A. (2017). The Eocene-Oligocene Otuma depositional sequence (East Pisco basin, Peru): paleogeographic and paleoceanographic implications of new data. *Boletín de la Sociedad Geológica del Perú*, *112*, 14–38.

Di Celma, C., Malinverno, E., Bosio, G., Collareta, A., Gariboldi, K., Gioncada, A., … Bianucci, G. (2017). Sequence stratigraphy and paleontology of the upper Miocene Pisco Formation along the western side of the lower Ica valley (Ica Desert, Peru). *Rivista Italiana di Paleontologia e Stratigrafia*, *123*, 255–274. doi:10.13130/2039-4942/8373

Di Celma, C., Malinverno, E., Bosio, G., Gariboldi, K., Collareta, A., Gioncada, A., … Bianucci, G. (2018a). Intraformational unconformities as a record of late Miocene eustatic falls of sea level in the Pisco Formation (southern Peru). *Journal of Maps*, *14*, 607–619. doi:10.1080/17445647.2018.1517701

Di Celma, C., Malinverno, E., Cantalamessa, G., Gioncada, A., Bosio, G., Villa, I. M., … Bianucci, G. (2016a). Stratigraphic framework of the late Miocene Pisco Formation at Cerro Los Quesos (Ica Desert, Peru). *Journal of Maps*, *12*, 1020–1028. doi:10.1080/17445647.2015.1115783

Di Celma, C., Malinverno, E., Collareta, A., Bosio, G., Gariboldi, K., Lambert, O., … Bianucci, G. (2018b). Facies analysis, stratigraphy and marine vertebrate assemblage of the lower Miocene Chilcatay Formation at Ullujaya (Pisco Basin. *Peru). Journal of Maps*, *14*, 257–268. doi:10.1080/17445647.2018.1456490

Di Celma, C., Malinverno, E., Gariboldi, K., Gioncada, A., Rustichelli, A., Pierantoni, P. P., … Bianucci, G. (2016b). Stratigraphic framework of the late Miocene to Pliocene Pisco Formation at Cerro Colorado (Ica Desert, Peru). *Journal of Maps*, *12*, 515–529. doi:10.1080/17445647.2015.1047906

Dunbar, R. B., Marty, R. C., & Baker, P. A. (1990). Cenozoic marine sedimentation in the Sechura and Pisco basins, Peru. *Palaeogeography Palaeoclimatology Palaeoecology*, *77*, 235–261. doi:10.1016/0031-0182(90)90179-B

Einsele, G. (1998). Event stratigraphy: Recognition and interpretation of sedimentary event horizons. In P. Doyle, & M. R. Bennet (Eds.), *Unlocking the stratigraphical record: Advances in modern stratigraphy* (pp. 145–193). Chichester: Wiley.

Esperante, R., Brand, L. R., Chadwick, A. V., & Poma, O. (2015). Taphonomy and paleoenvironmental conditions of deposition of fossil whales in the diatomaceous sediments of the Miocene/Pliocene Pisco Formation, southern Peru – a new fossil-Lagerstätte. *Palaeogeography Palaeoclimatology Palaeoecology*, *417*, 337–370. doi:10.1016/j.palaeo.2014.09.029

Gariboldi, K., Bosio, G., Malinverno, E., Gioncada, A., Di Celma, C., Villa, I. M., … Bianucci, G. (2017). Biostratigraphy, geochronology and sedimentation rates of the upper Miocene Pisco Formation at two important marine vertebrate fossil-bearing sites of southern Peru. *Newsletters on Stratigraphy*, *50*, 417–444. doi:10.1127/nos/2017/0345

Gariboldi, K., Gioncada, A., Bosio, G., Malinverno, E., Di Celma, C., Tinelli, C., … Bianucci, G. (2015). The dolomite nodules enclosing fossil marine vertebrates in the East Pisco Basin, Peru: Field and petrographic insights into the Lagerstätte formation. *Palaeogeography, Palaeoclimatology, Palaeoecology*, *438*, 81–95. doi:10.1016/j.palaeo.2015.07.047

Gioncada, A., Collareta, A., Gariboldi, K., Lambert, O., Di Celma, C., Bonaccorsi, E., … Bianucci, G. (2016). Inside baleen: Exceptional microstructure preservation in a late

Miocene whale skeleton from Peru. *Geology*, *44*, 839–842. doi:10.1130/G38216.1

Gioncada, A., Gariboldi, K., Collareta, A., Di Celma, C., Bosio, G., Malinverno, E., … Bianucci, G. (2018a). Looking for the key to preservation of fossil marine vertebrates in the Pisco Formation of Peru: New insight from a small dolphin skeleton. *Andean Geology*, *45*, 379–398. doi:10.5027/andgeoV45n3-3122

Gioncada, A., Petrini, R., Bosio, G., Gariboldi, K., Collareta, A., Malinverno, E., … Bianucci, G. (2018b). Insights into the diagenetic environment of fossil marine vertebrates of the Pisco Formation (late Miocene, Peru) from mineralogical and Sr-isotope data. *Journal of South American Earth Sciences*, *81*, 141–152. doi:10.1016/j.jsames.2017.11.014

Hampel, A., Kukowski, N., Bialas, J., & Huebscher, C. (2004). Ridge subduction at an erosive margin: The collision zone of the Nazca Ridge in southern Peru. *Journal of Geophysical Research*, *109*. doi:10.1029/2003JB002593

Hansen, K. S. (1999). Development of a prograding carbonate wedge during sea level fall: Lower Pleistocene of Rhodes, Greece. *Sedimentology*, *46*, 559–576. doi:10.1046/j.1365-3091.1999.00238.x

Hernández-Molina, F. J., Fernández-Salas, L. M., Lobo, F., Somoza, L., Díaz-del-Río, V., & Alveirinho Dias, J. M. (2000). The infralittoral prograding wedge: A new large-scale progradational sedimentary body in shallow marine environments. *Geo-Marine Letters*, *20*, 109–117. doi:10.1007/s003670000040

Hsu, J. T. (1992). Quaternary uplift of the Peruvian coast related to the subduction of the Nazca Ridge: 13.5 to 15.6 degrees south latitude. *Quaternary International*, *15–16*, 87–97. doi:10.1016/1040-6182(92)90038-4

Lambert, O., Bianucci, G., Post, K., de Muizon, C., Salas-Gismondi, R., Urbina, M., & Reumer, J. (2010). The giant bite of a new raptorial sperm whale from the Miocene epoch of Peru. *Nature*, *465*, 105–108. doi:10.1038/nature09067

Lambert, O., Bianucci, G., Urbina, M., & Geisler, J. H. (2017a). A new inioid (Cetacea, Odontoceti, Delphinidae) from the Miocene of Peru and the origin of modern dolphin and porpoise families. *Zoological Journal of the Linnean Society*, *179*, 919–946. doi:10.1111/zoj.12479

Lambert, O., Collareta, A., Landini, W., Post, K., Ramassamy, B., Di Celma, C., … Bianucci, G. (2015). No deep diving: Evidence of predation on epipelagic fish for a stem beaked whale from the late Miocene of Peru. *Proceedings of the Royal Society of London Part B: Biological Sciences*, *282*, article no. 20151530. doi:10.1098/rspb.2015.1530

Lambert, O., de Muizon, C., Malinverno, E., Di Celma, C., Urbina, M., & Bianucci, G. (2018). A new odontocete (toothed cetacean) from the early Miocene of Peru expands the morphological disparity of extinct heterodont dolphins. *Journal of Systematic Palaeontology*, *16*, 981–1016. doi:10.1080/14772019.2017.1359689

Lambert, O., Martínez-Cáceres, M., Bianucci, G., Di Celma, C., Salas-Gismondi, R., Steurbaut, E., … de Muizon, C. (2017b). Earliest Mysticete from the late Eocene of Peru sheds new light on the origin of baleen whales. *Current Biology*, *27*, 1535–1541. doi:10.1016/j.cub.2017.04.026

Landini, W., Altamirano-Sierra, A., Collareta, A., Di Celma, A., Urbina, M., & Bianucci, G. (2017a). The late Miocene elasmobranch assemblage from Cerro Colorado (Pisco Formation, Peru). *Journal of South American Earth Sciences*, *73*, 168–190. doi:10.1016/j.jsames.2016.12.010

Landini, W., Collareta, A., Di Celma, C., Malinverno, E., Urbina, M., & Bianucci, G. (2019). The early Miocene elasmobranch assemblage from Zamaca (Chilcatay Formation, Peru). *Journal of South American Earth Sciences*. doi:10.1016/j.jsames.2018.08.004

Landini, W., Collareta, A., Pesci, F., Di Celma, C., Urbina, M., & Bianucci, G. (2017b). A secondary nursery area for the copper shark *Carcharhinus brachyurus* from the late Miocene of Peru. *Journal of South American Earth Sciences*, *78*, 164–174. doi:10.1016/j.jsames.2017.07.003

Leithold, E. L., & Bourgeois, J. (1984). Characteristics of coarse-grained sequences deposited in nearshore, wave-dominated environments-examples from the Miocene of south-west Oregon. *Sedimentology*, *31*, 749–775. doi:10.1111/j.1365-3091.1984.tb00884.x

León, W., Aleman, A., Torres, V., Rosell, W., & De la Cruz, O. (2008). Estratigrafía, sedimentología y evolución tectónica de la cuenca Pisco Oriental. *Boletín INGEMMET (Serie D)*, *27*, 1–144.

MacEachern, J. A., & Pemberton, S. G. (1992). Ichnological aspects of Cretaceous shoreface successions and shoreface variability in the Western Interior Seaway of North America. In S. G. Pemberton (Ed.), *Applications of Ichnology to Petroleum Exploration* (pp. 57–84). Calgary, AB: SEPM Core Workshop No. 17.

Macharé, J., & Ortlieb, L. (1992). Plio-Quaternary vertical motions and the subduction of the Nazca Ridge, central coast of Peru. *Tectonophysics*, *205*, 97–108. doi:10.1016/0040-1951(92)90420-B

Martinez-Caceres, M., Lambert, O., & de Muizon, C. (2017). The anatomy and phylogenetic affinities of *Cynthiacetus peruvianus*, a large *Dorudon*-like basilosaurid (Cetacea, Mammalia) from the late Eocene of Peru. *Geodiversitas*, *39*, 7–163. doi:10.5252/g2017n1a1

Marx, F. G., Collareta, A., Gioncada, A., Post, K., Lambert, O., Bonaccorsi, E., … Bianucci, G. (2017b). How whales used to filter: Exceptionally preserved baleen in a Miocene cetotheriid. *Journal of Anatomy*, *231*, 212–220. doi:10.1111/joa.12622

Marx, F. G., Lambert, O., & de Muizon, C. (2017a). A new Miocene baleen whale from Peru deciphers the Dawn of cetotheriids. *Royal Society Open Science*, *4*, 170560. doi:10.1098/rsos.170560

Massari, F., & D'Alessandro, A. (2012). Facies partitioning and sequence stratigraphy of a mixed siliciclastic-carbonate ramp stack in the Gelasian of Sicily (S Italy): a potential model for icehouse, distally-steepened heterozoan ramps. *Rivista Italiana di Paleontologia e Stratigrafia*, *118*, 503–534. doi:10.13130/2039-4942/6017

Mukasa, S. B., & Henry, D. J. (1990). The San Nicolás batholith of coastal Peru: Early Palaeozoic continental arc or continental rift magmatism? *Journal of the Geological Society, London*, *147*, 27–39. doi:10.1144/gsjgs.147.1.0027

NACSN (North American Commission on Stratigraphic Nomenclature). (2005). North American stratigraphic code. *American Association of Petroleum Geologists Bulletin*, *89*, 1547–1591. doi:10.1306/07050504129

Patruno, S., Hampson, G. J., Jackson, C. A.-L., & Dreyer, T. (2015). Clinoform geometry, geomorphology, facies character and stratigraphic architecture of a sand-rich subaqueous delta: Jurassic Sognefjord Formation, offshore Norway. *Sedimentology*, *62*, 350–388. doi:10.1111/sed.12153

Pemberton, S. G., & MacEachern, J. A. (1997). The ichnological signature of storm deposits: The use of trace fossils in event stratigraphy. In C. E. Brett, & G. C. Baird (Eds.), *Paleontological events, stratigraphical, ecological and*

evolutionary implications (pp. 73–109). New York: Columbia University Press.

Pomar, L., & Kendall, C. G. S. C. (2008). Architecture of carbonate platforms: A response to hydrodynamics and evolving ecology. In J. Lukasik, & A. Simo (Eds.), *Controls on carbonate platform and reef development* (pp. 187–216). Tulsa: SEPM, Special Publication, 89. doi:10.2110/pec.08.89.0187.

Pomar, L., & Tropeano, M. (2001). The Calcarenite di Gravina Formation in Matera (southern Italy): new insights for coarse-grained, large scale, cross-bedded bodies encased in offshore deposits. *American Association of Petroleum Geologists Bulletin*, *85*, 661–689. doi:10.1306/8626C979-173B-11D7-8645000102C1865D.

Pomar, L., Aurell, M., Bádenas, B., Morsilli, M., & Al-Awwad, S. F. (2015). Depositional model for a prograding oolitic wedge, Upper Jurassic, Iberian basin. *Marine and Petroleum Geology*, *67*, 556–582. doi: 10.1016/j.marpetgeo.2015.05.025

Rustichelli, A., Di Celma, C., Tondi, E., Baud, P., & Vinciguerra, S. (2016b). Fibrous gypsum veins as diffuse features and within fault zones: The case study of the Pisco Basin (Ica desert, southern Peru). *Journal of the Geological Society, London*, 173, 405–418. doi:10.1144/jgs2015-084

Rustichelli, A., Di Celma, C., Tondi, E., & Bianucci, G. (2016a). Deformation within the Pisco basin sedimentary record (southern Peru): Stratabound orthogonal vein sets and their impact on fault development. *Journal of South American Earth Sciences*, *65*, 79–100. doi:10.1016/j.jsames.2015.11.002

Saillard, M., Hall, S. R., Audin, L., Farber, D. L., Regard, V., & Hérail, G. (2011). Andean coastal uplift and active tectonics in southern Peru: ^{10}Be surface exposure dating of differentially uplifted marine terrace sequences (San Juan de Marcona, ~15.4°S). *Geomorphology*, *128*, 178–190. doi:10.1016/j.geomorph.2011.01.004

Thornburg, T. M., & Kulm, L. D. (1981). Sedimentary basins of the Peru continental margin: Structure, stratigraphy, and Cenozoic tectonics from 6°S to 16°S latitude. In L. D. Kulm, J. Dymond, E. J. Dasch, & D. M. Hussong (Eds.), *Nazca plate: Crustal formation and Andean convergence* (pp. 393–422). Memoir: Geological Society of America, 154.

Viveen, W., & Schlunegger, F. (2018). Prolonged extension and subsidence of the Peruvian forearc during the Cenozoic. *Tectonophysics*, *730*, 48–62. doi:10.1016/j.tecto.2018.02.018

Zecchin, M., Catuneanu, O., & Caffau, M. (2019). Wave-ravinement surfaces: Classification and key characteristics. *Earth-Science Reviews*, *188*, 210–239. doi:10.1016/j.earscirev.2018.11.011

Zonneveld, J.-P., & Moslow, T. F. (2004). Exploration potential of the Falher G shoreface conglomerate trend: Evidence from outcrop. *Bulletin of Canadian Petroleum Geology*, *52*, 23–38. doi:10.2113/52.1.23